A quantum-inspired sensor consolidation measurement approach for cyber-physical systems.

MEKALA, M.S., SRIVASTAVA, G., GANDOMI, A.H., PARK, J.H. and JUNG, H.-Y.

2024

A Quantum-Inspired Sensor Consolidation Measurement Approach for Cyber-Physical Systems

M S Mekala, *Member, IEEE,* Gautam Srivastava, *Senior Member, IEEE,* Amir H Gandomi, Ju H. Park, *Senior Member, IEEE,* and Ho-Youl Jung, *Senior Member, IEEE,*

Abstract—Cyber-Physical System (CPS) devices interconnect to grab data over a common platform from industrial applications. Maintaining immense data and making instant decision analysis by selecting a feasible node to meet latency constraints is challenging. To address this issue, we design a quantum-inspired online node consolidation (QONC) algorithm based on a time-sensitive measurement reinforcement system for making decisions to evaluate the feasible node, ensuring reliable service and deploying the node at the appropriate position for accurate data computation and communication. We design the Angular-based node position analysis method to localize the node through rotation and t-gate to mitigate latency and enhance system performance. We formalize the estimation and selection of the feasible node based on quantum formalization node parameters (node contiguity, node optimal knack rate, node heterogeneity, probability of fusion variance error ratio). We design a fitness function to assess the probability of node fitness before selection. The simulation results convince us that our approach achieves an effective measurement rate of performance index by reducing the average error ratio from 0.17-0.22, increasing the average coverage ratio from 29% to 42%, and the qualitative execution frequency of services. Moreover, the proposed model achieves a 74.3% offloading reduction accuracy and a 70.2% service reliability rate compared to state-of-the-art approaches. Our system is scalable and efficient under numerous simulation frameworks.

Index Terms—Quantum computing, Node contiguity rate, Node knack measurement index, Machine learning, Hadamard gate.

I. INTRODUCTION

Cyber-Physical Systems (CPS), which combine sensor frameworks, and computational and physical components, are employed to control automated environments and fulfill the demands of the Industry 4.0 paradigm [1]. This paradigm entails coordinating computation, communication, and control mechanisms through conditional probabilistic networks or graph theory. However, the lack of integration among decision models within the environment introduces varying levels of complexity. This may consume abnormal energy to maintain the network services and causes an unusual learning ratio through classical computing-based machine learning techniques. Moreover, data generation is increasing as CPS application deployments increase. The lack of adequate edge computing environments hinders achieving optimal quality-of-services (QoS) for CPS applications. A detailed investigation report is presented in [2] regarding the QOS optimization perspective; In this survey, the authors provide a concise overview of the research gaps in areas such as latency, energy usage, reliability, and privacy concerning CPS applications. The next-generation network demands (enormous resources and security standards) may resolve using learning models with a backbone of quantum computing [3]. Theoretical quantum computing is an optimal solution for meeting the needs of 5G communication networks by cloning the quantum mechanism [4] on network nodes to optimize the communication and computation overhead. As a result, designing a quantum decision-making method is challenging, but it may help choose the right node to execute the offloading services at the network edge.

Sensor localization and its operational decisions are prominent factors for enhancing the lifetime of the CPS framework. Let us assume $s \times a$ network area is considered to formulate the listed issues, where s refers to a set of sensors and a refers to a set of anchors. The main challenge is sensor classification based on their activities through a quantum mechanism by considering each cycle's data. Selection of activities such as inactive (switch-off) the sensor and classification of low area and high coverage sensors impact the network service reliability, network lifetime, and network energy usage. The node localization technologies are primarily categorized into two types; first, range-based approaches [5], which effectively work based on Angle of Arrival (AoA) [6], Time of Arrival (ToA) [7], Time Difference of Arrival (TDoA). Second, range-free-based approaches [8], [9] work effectively based on connectivity information among neighbouring devices. The existing methods effectively execute the services through classical computing, which is time-consuming. Recently, an automated vehicle network technology has received attention globally; therefore, we focused on designing a range-free approach based on quantum machine learning to optimize the overhead of communication and computation services due to the vast

M S Mekala is with school of computing, Robert Gordon University, Garthdee road, aberdeen, AB10 7QB, scotland, UK. (E-mail: ms.mekala@rgu.ac.uk & msmekala@yu.ac.kr).

Ho-Youl Jung is with department of Information and Communication Engineering,Yeungnam University, Gyeongsan 38544, Korea as well as RLRC for Autonomous Vehicle Parts and Materials Innovation, Yeungnam University, Gyeongsan 38544, Korea (E-mail: hoyoul@yu.ac.kr (corresponding author)).

Gautam Srivastava is with the Dept. of Math and Computer Science, Brandon University, Brandon, Canada and the Research Centre for Interneural Computing, China Medical University, Taichung, Taiwan as well as with the Dept. of Computer Science and Math, Lebanese American University, Beirut 1102, Lebanon. (E-mail: srivastavag@brandonu.ca)

Amir H Gandomi is with Faculty of Engineering and Information Technology, University of Technology Sydney, Ultimo, NSW 2007, Australia (e-mail: gandomi@uts.edu.au), and University Research and Innovation Center (EKIK), Óbuda University, 1034 Budapest, Hungary

Ju H. Park, Department of Electrical Engineering, Yeungnam University, Gyeongsan 38544, Korea. (E-mail: jessie@ynu.ac.kr).

Corresponding Author: Gautam Srivastava

TABLE I: Tools and technologies comparative study; Quantum Programming Studies (QPS), Quantum Development Kit

Tool	Parameters							
	Toolkit	Opensource	Simulation	Real Implementation	Built-in Algorithms	Gate Scheduling	Coding	Matrix Support
QPS	✓	✓	✓	✗	✓	✓	Javascript	✓
Qubit4MATLAB	✗	✓	✓	✗	✓	✓	MATLAB	✓
Cirq	✓	✓	✓	✓	✓	✓	Python	✓
Qiskit	✓	✓	✓	✓	✓	✓	Python	✓
QDK	✓	✓	✓	✗	✓	✓	Python,Q#	✓

usage of smart devices.

Therefore, there is a need to design and develop an algorithm for continuous updates of residual-energy level, sensor contiguity rate, optimal knock rate, and novel distance measurement. The algorithm iteratively collects node-centric data after each cycle helps to make an accurate decision, but it is an NP-hard problem. However, few metaheuristic algorithms developed to resolve these issues [10]. For instance, Genetic Algorithms (GA), Ant Colony Optimization (ACO), Particle Swarm Optimization (PSO), and Gravitational Search Algorithm (GSA) are pretty well metaheuristic algorithms that are widely used in CPS applications [11] but require a long time to compute and process. Another drawback is that extending the problem's search space requires converging on optimal solutions. In this regard, we design a quantum-inspired multi-objective data fusion measurement approach to enhance the sensor state's quantization ratio by leveraging the sensor coverage range, efficiency, and specific node-centric metrics.

Motivation: Maintaining and analyzing immense amounts of data to make an instant decision by an edge server or vehicle node is an essential task in the vehicular network. We considered an abnormal scenario where the computation-intensive tasks offload to the suitable server or device to meet the application deadline. In this process, a crucial phase is selecting a potential device and locating a device in the right place. In line with this issue, two algorithms are developed based on quantum theory, irrespective of classical machine learning. The selection and localization mechanism is divided into three tasks (measuring node-centric parameters, quantum state estimation, and data fusion optimization). In our constructions, Algorithm 1 assesses the rotation angle magnitude to assess the rotation direction of the vehicle and distance based on node fitness, node degree, normalization value, and qubit register probability for effective location analysis subject to data fusion (Theorem 2). Consequently, Algorithm 2 assesses node selection based on quantum state estimation (Theorem 1) subject to node contiguity, node optimal knack rate, and node heterogeneity parameters for the initial selection of feasible nodes. Moreover, we design a probability-based fitness function to finalize the node selection based on quantum state estimation, which can be observed in Fig. 1. Simultaneously, RSU/server localization is formulated by extending the above measurements along with directionality. In this regard, we design an angular-based node position analysis method to localize the node through rotation and t-gate to mitigate the latency and enhance the system performance. MATLAB

and Qiskit are considered to estimate the probability of each vehicle state. The node consolidation issue is formulated by dividing it into two-sub tasks (node selection and deployment) subject to the probabilities of qubits, quantum state, node contiguity, node optimal knack rate, node heterogeneity, and probability of node fitness. Our contributions are listed as follows:

1) Develop a quantum-inspire online node consolidation (QONC) algorithm based on a time-sensitive measurement reinforcement system through a quantum-inspired node-centric measurement method and fitness function to evaluate the feasible node for ensuring reliable service by deploying the node at the appropriate position for accurate data computation and communication.
2) Develop an angular-based node position analysis method to localize the node through rotation and T-gate to mitigate the latency and enhance the system performance.
3) Conduct simulations based on MATLAB with QUBIT V5.8 and Qiskit to assess the proposed system performance

Table I provides a brief examination and amendment of the functionalities of the tools and technologies, offering valuable assistance to research scholars. Section II briefly describes research gaps and issues of extant approaches. Section IV describes the proposed system and its mathematical model with a novel algorithm in detail. Section V evaluates the outcome examination, and Section VI concludes the manuscript.

II. RELATED WORK

Recent research works are examined in line with the article's objectives which are classified into two subsections.

A. Accurate data fusion importance based on quantum theory

Usually, effective data fusion impacts system performance by optimizing the energy consumption, data compression, and transmission overhead of CPS systems; since all report to the sink node. We believe that making the sensors inactive, which is not feasible to fulfill the system requirements, impacts the communication and computation overhead of the system. Therefore, selecting the abnormal sensor, device, or node based on node-centric measurements is challenging. In line with this motivation, we investigated recently published articles to resolve this issue based on quantum theory by estimating each node's probability state.

In [12], a butterfly quantum network is developed to estimate the state of each qubit using communication channel

TABLE II: Related works brief in line with article objectives

References	Objectives									
	Node selection	Qubit-state estimation	Channel analysis	Angle estimation	Noise tolerence	Latency	Coverage analysis	Resource capacity	Node fitness	Dimensions degree
[12], [13]	✓	✓	✓	✗	✓	✓	✗	✓	✗	✗
[14]	✓	✓	✓	✗	✗	✓	✗	✓	✗	✗
[8]	✓	✓	✓	✗	✗	✓	✓	✓	✓	✗
[9]	✓	✓	✗	✓	✗	✓	✗	✗	✗	✓
[15]	✓	✓	✓	✗	✓	✓	✓	✗	✗	✓
[16], [17]	✓	✓	✓	✗	✗	✓	✓	✗	✓	✓
[18]	✓	✗	✓	✗	✓	✓	✓	✓	✗	✓
[19], [20], [21], [22], [23]	✗	✗	✓	✗	✓	✓	✓	✓	✗	✓
[24]	✓	✓	✓	✗	✓	✓	✗	✓	✗	✗
QONC	✓	✓	✓	✓	✓	✓	✓	✓	✓	✓

auxiliary data in the process of target node analysis. A quantum cooperative multicast (QCM) model is developed to optimize the network transmission losses [13]. However, these models are not optimal for lightweight communication networks.

In [14], efficient resource allocation is designed based on quantum states using the Quantum-based particle swarm optimization method. The author concentrated on diminishing the network iteration to achieve high performance. In [8], the node density and node coverage rate-based swarm optimization algorithm is designed to resolve the node deployment using quantum theory (NDQ) and is treated as A3. In continuation, a Quantum-inspired green communication framework for Energy Balancing in sensor-enabled CPS systems (Q-EBIT) is developed using a single receiving angle to localize the node in the network [9], and it is treated as A2. In [15], node energy consumption and hop count attributes are considered with heuristic and deterministic methods designed based on quantum theory to resolve the CPS framework node searching issues. Subsequently, a quantum-inspired genetic algorithm is proposed called quantum approximate optimization algorithm (QAOA) for effective service execution based on policy gradient learning strategy to resolve the device-centric issues based on hypothesis data collected and processed asynchronously to improve the system performance accuracy [16] and is treated as A1. In [17], the researchers design a machine learning architecture-based novel quantum service allocation model to address the next-generation network gaps. This algorithm called the qubit-preserved shortest path algorithm (DQRA), assesses the reward function to increase the service execution rate in each routing window.

B. Sensor selection approaches

In [18], the authors measure an Expected hop Progress (EP) based distance through two nodes. However, the system is unsuitable for complex systems because of the longer-range coverage rate. In [19], researchers develop a novel scheduler with window constraints for routers to address communication issues related to router allocation problems and emergency data allocation. The scheduler shows promising results, achieving an average running time of 0.209 seconds. However, it is important to consider the complexity aspect, as the model includes four designed algorithms. In

[20], researchers develop a role-aware hypergraph based on hypergraphs and an attention mechanism to consolidate the nodes' role and achieve a 12.1% accuracy improvement in node classification. In [21], the researchers design an Anchor Pairs Condition (APC) analysis method to assess the distance relation among anchor nodes for effective localization. Those nodes are classified as optimal/suboptimal based on different distance measurements. In [22], the researchers design a novel localization method for node localization by measuring the horizontal distance based on the angle of an arrived signal. In [23], the authors develop a power-efficient node Localization (PENL) approach based on Neural Network (NN) for effective distance measurement among devices, which does not depend on several hops counts. It measures the distance based on an anisotropic signal. However, the extent of algorithm performances is degenerative due to many node-centric factors, especially in sparse networks. Therefore, a robust range-free localization algorithm is essential for effective autonomous vehicle orchestration based on quantum theory.

III. PRELIMINARIES

The authors and the research community have shown increasing interest in quantum computing in recent years, as it offers potential improvements in performance metrics such as latency and reliability while maintaining low complexity similar to classical models. However, selecting the appropriate implementation platform remains a challenging task. One notable option is the D-wave 2000Q[1], which boasts 2000 qubits. Additionally, IBM[2] has announced plans to release a machine based on 50 qubits by 2020, although it is still in the development phase. Moreover, each qubit resembles a super state and after measurement, the final state would be 0, 1 like a classical binary bit. A two-dimension state refer as $|0\rangle$, $|1\rangle$ and its each state probability (a, b) is normalized as $|a|^2 + |b|^2 = 1$ [25].

$$\begin{array}{l} State - 0 \rightarrow \\ State - 1 \rightarrow \end{array} \left[\begin{array}{c|c|c|c} a_{01} & a_{02} & \cdots & a_{0n} \\ b_{11} & b_{12} & \cdots & b_{1n} \end{array} \right] \quad (1)$$

[1]https://www.dwavesys.com/d-wave-two-system
[2]https://www-03.ibm.com/press/us/en/pressrelease/53374.wss
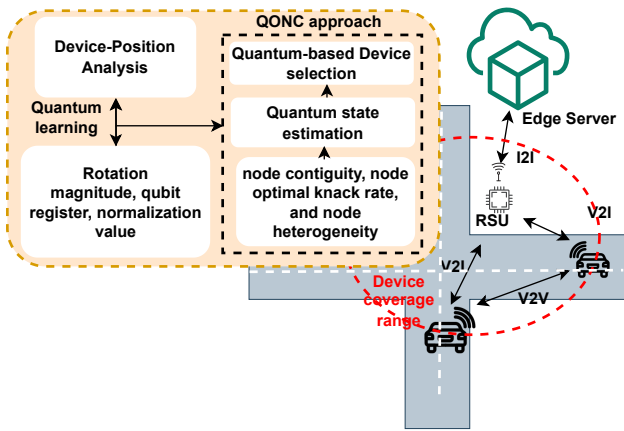
Fig. 1: System model

Assume a two ($n = 2$) bits quantum register with their state probabilities as follows.

$$|q_1\rangle = \frac{1}{\sqrt{2}}|0\rangle + \frac{1}{\sqrt{2}}|1\rangle$$

where $a = \frac{1}{\sqrt{2}}, b = \frac{1}{\sqrt{2}}$, the conditional probability is $|a|^2 + |b|^2 = 1$. Accordingly, $= \left|\frac{1}{\sqrt{2}}\right|^2 + \left|\frac{1}{\sqrt{2}}\right|^2 = \frac{1}{2} + \frac{1}{2} = 1$. The normalized sum of probabilities equals 1, and the measurement of the 3-qubit register proceeds as described below.

$$\overset{q_1}{\overset{\downarrow}{|\ 0}} \overset{q_2}{\overset{\downarrow}{0}} \overset{q_3}{\overset{\downarrow}{0}}\rangle = \frac{1}{\sqrt{2}}|0\rangle + \frac{1}{\sqrt{2}}|0\rangle + \frac{\sqrt{3}}{2}|0\rangle$$

here $a = \frac{1}{\sqrt{2}}, b = \frac{1}{\sqrt{2}}, c = \frac{\sqrt{3}}{2}$. The probability of three qubits is

$$= (abc)\,|000\rangle$$
$$= \left(\frac{1}{\sqrt{2}} \cdot \frac{1}{\sqrt{2}} \cdot \frac{\sqrt{3}}{2}\right)|000\rangle = \left(\frac{\sqrt{3}}{4}\right)|000\rangle$$

A. Communication model

In this paper, we have examined a similar experimental environment [26], [27]. To evaluate the signal-to-noise ratio, we have employed the default method $\delta_i^{com} = \left[(tp_i^{com} g_i^{com})/\sigma^2\right]$, where tp_i^{com} represents the transmission power with limits defined as $tp_i^{com} \epsilon \left[tp_i^{com,min}, tp_i^{com,max}\right]$, g_i^{com} represents the channel gain, σ^2 denotes the channel noise, and ω_i^{com} represents the bandwidth. The transmission rate between the node and RSU is defined using the Shannon-Hartley formula as $s_{i,i+1|k}^{com} = \omega_i^{com} \log_2\left(1 + \delta_i^{com}\right)$. The probability of the communication channel is updated based on the probabilities of transmission rate, node/vehicle direction, coverage, and angle, as expressed by $\psi_{l,l+1|k} \leftarrow \rho$ [transmission, direction, coverage, angle]. The objective is to ensure that this probability is below a threshold value to achieve the desired goals.

B. Computation model

The execution of services typically occurs locally on the On-Board Unit (OBU). However, when dealing with computation-intensive tasks, the services are offloaded to a server or cloud, which is a fundamental strategy. As a result, the latency of local computations is defined as

$$\tau_i^{loc} = \frac{\text{required resources for service execution}}{\phi_l(\text{resources of } l^{th} \text{ OBU or node})}$$

The definition of server-side computation latency is as follows, and it must not exceed the threshold value. i.e, $\tau_{l,l+1|k} \leq \tau^{thr}$.

$$\tau_i^{l,l+1|k} = \frac{\text{Size of the service(bits)}}{s_{i,i+1|k}^{com}} + \tau_i^{loc}$$

C. Problem formulation

Node consolidation involves the validation of a node for inclusion within a framework that facilitates data fusion. This process is crucial for ensuring the precise design of a decision-making system in autonomous vehicle systems. As next-generation automated vehicle frameworks become prevalent, they accommodate a vast number of active edge devices, actuators, and the Internet of Things (IoT). These multi-dimensional physical spaces present resource capacity challenges. Additionally, traditional machine learning techniques fall short of meeting the learning requirements of industrial applications due to limited data analytics, exploration, and exploitation capabilities. To fulfill these requirements, the service optimization problem can be formulated as follows:

$$min \sum \rho\left(\zeta_{l,l+1|k}\right) \cdot \rho\left(\tau_{l,l+1|k}\right) + \left(1 - \rho\left(\zeta_{l,l+1|k}\right)\right)$$
$$+ \left[\rho\left(\phi_{l,l+1|k}\right) \cdot \rho\left(\tau_{l,l+1|k}\right) + \left(1 - \rho\left(\phi_{l,l+1|k}\right)\right) \cdot \rho\left(\tau_{l,l+1|k}\right)\right] \tag{2}$$

Subject to:

C_1 : Offloading decision rate $\zeta_{l,l+1|k} \leq \zeta^{thr}$

C_2 : Resource potentiality $\phi_{l,l+1|k} \leq \phi^{thr}$

C_3 : Channel (direction, transmission, coverage, angle) $\psi_{l,l+1|k} \leq \psi^{thr}$

C_4 : Qubit state-error probability $O_s^{pe} \leq O_{s,pe}^{thr}$

C_5 : Fusion variance $\chi_s^{pe} \leq \chi_{s,pe}^{thr}$

The primary objective of this article is to address the node selection challenge in service offloading, with a specific focus on achieving low latency and efficient resource utilization, where ρ ensures the probability of each variable. Several recent publications and researchers have made notable efforts to tackle this problem satisfactorily. Our approach involves formulating the optimization problem by evaluating the qubit state probability of each dimension, and angle measurement and considering the impact of vehicle mobility on network performance. The node selection and deployment problem is formulated using theoretical and mathematical principles. A set of constraints is defined, and it is crucial to ensure that all these variables remain below their respective threshold values. However, due to the inclusion of binary decision bits, the optimization problem becomes non-convex, resulting in an exponential increase in function complexity (likely 2^N) with the size of space represented by C_1, C_2 and C_5. These

factors are evident that this issue is similar to the NP-Hard problem. Moreover, the article highlights the quantum computing mechanism in line with the objectives.

IV. QUANTUM-INSPIRED SENSOR CONSOLIDATION MECHANISM

Let us assume, a CPS framework enables a set of randomly deployed sensors S in $a \times a$ network area with density $\rho = \frac{S}{(a \times a)}$, R communication radius. Where s_e^l, $(l = 1, 2, \cdots, L)$ denotes a set of GPS-enabled sensors called *active-nodes*, and s_c^k, $(k = 1, 2, \cdots, K)$ denotes a set of *hyper nodes* $s_c = S - s_e$ that may perform both relay services and computation services as per the demand where the service arrival rate is λ_i for l^{th} vehicle. The sensor cluster is formulated based on their distance, where paired sensors' reliability is essential to execute the services with low latency by following a novel offloading strategy with a measurement index. For more information please refer [24], [28]. This section further subdivides based on context such as quantum angular theory for node coordinates analysis, fusion variance measurement, node selection strategy, node mobility impact on node selection, and proposed approach complexity.

A. Quantum angular-based node coordinates analysis

Reliability plays an important role to establish the communication and computation path by selecting the sensor pair which have the maximum high-reliability value including relay sensors. The service reliability is measured with Eq. 3.

$$\alpha_{l,l+1}^k = \frac{1}{S} \times \frac{d_{l,l+1}}{(r_{l,k} + r_{k,l+1})} \; ; \forall \; 0 < \alpha_{l,l+1}^k \leq R \quad (3)$$

Deriving the possible location of the relay node is essential since its location coordinates and location angle are unaware. Let us assume that two active sensors (S_l^e, S_{l+1}^e) are deployed with a maximum communication range of $r_{l,k}^i R$, $r_{l+1,k}^i R$ respectively. The distance between the relay node and an active node is calculated using Eq. 4.

$$d_{l,k} = \int\limits_0^{\theta_{l+1,k}} \frac{r_{l,k} \cdot \alpha_{l,l+1}^k}{\sin \theta_l^k} \quad (4)$$

The $\vartheta \; (\vartheta \subset (-\pi, \pi])$ denotes the phase of each qubit; how-
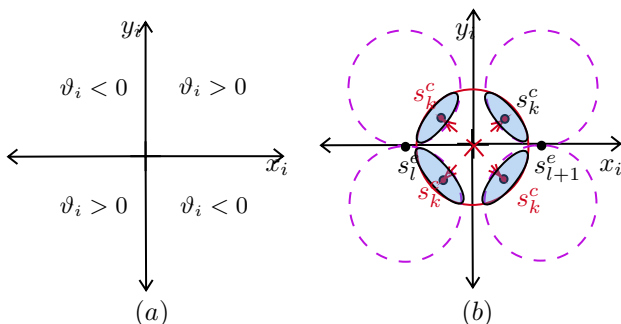

Fig. 2: Quadratic place of the sensor. a) 4 phases of the sensor b) rotation angle-based sensor localization

ever, the ith qubit phase is $\vartheta_i = \arctan \left(x_i / y_i \right)$. Each qubit phase position may occupy any quarter among the four as follows. Qubit phase position ϑ_i is illustrated in Figure 2. The Quantum-based Sensor Angle Position (QSAP) measurement index helps to place the regular node at the right place by estimating the feasibility of each qubit concerning the sensor position. The quantum rotation gate plays an important role in qubit calculation and is derived as follows. The following formula represents a qubit which rotates θ_l^k degrees from the original vector $(x_i, y_i) \rightarrow \left(x_i', y_i' \right)^T$.

$$\begin{bmatrix} x_i' \\ y_i' \end{bmatrix} = \begin{pmatrix} \cos\left(\theta_l^k\right) & -\sin\left(\theta_l^k\right) \\ \sin\left(\theta_l^k\right) & \cos\left(\theta_l^k\right) \end{pmatrix} \begin{bmatrix} x_i \\ y_i \end{bmatrix} \quad (5)$$

θ_l^k is the rotation angle, and it is calculated with Eq. 6

$$\theta_l^k = \hbar \times p(x_i, y_i) \quad (6)$$

where τ denotes iterations count, $\hbar = 4 \times \exp\left(\frac{-\tau}{\tau^{\max}}\right)$ represents rotation step to control the rotation speed; and τ^{max} denotes maximum number of iterations. The calculation of the node direction is highly essential and is defined as the function $p(x_i, y_i)$ as follows.

$$p(x_i, y_i) = \frac{1}{r_{l,k} + r_{l+1,k}} \times \left(\frac{d_{l,k}^{be}}{d_{l,k}^{pre}} \right) \left(\vartheta_{l,k}^{be} - \vartheta_{l,k}^{pre} \right) \quad (7)$$

where

$$d_{l,k}^{be} = \frac{x_{l,k}^{be}}{y_{l,k}^{be}} \times d_{l,l+1}^{be} \cos\theta - d_{l,l+1}^{be} \sqrt{\cos_{be}^2 \theta - \left(1 - R_{l+1}^2\right)}$$

$$d_{l,k}^{pre} = \frac{x_{l,k}^{pre}}{y_{l,k}^{pre}} \times d_{l,l+1}^{pre} \cos\theta - d_{l,l+1}^{pre} \sqrt{\cos_{pre}^2 \theta - \left(1 - R_{l+1}^2\right)}$$

$$\vartheta_{l,k}^{be} = \arctan\left(x_{l,k}^{be} / y_{l,k}^{be}\right)$$

$$\vartheta_{l,k}^{pre} = \arctan\left(x_{l,k}^{pre} / y_{l,k}^{pre}\right)$$

The $d_{l,k}^{be}, d_{l,k}^{pre}, \vartheta_{l,k}^{be}, \vartheta_{l,k}^{pre}$ are the probability of the ith qubit best and predicted resolved coordinates, respectively. Finally, if $p(x_i, y_i) < 0$, the θ_l^k, $(k = 1, 2, \cdots, K)$ rotates clockwise; otherwise, it rotates anticlockwise to place the sensor node at the reliable position.

Let us define the qubit of every sensor S and assume every qubit is an attribute to assess the state of every sensor—that is, $Q = (q_1, q_2, \cdots, q_s, \cdots, q_n)$, $\therefore s_l^e \cup s_c^k \subseteq S$.

$$q_s = \begin{pmatrix} x_1 & | & x_2 & | & x_3 & \cdots & | & x_n \\ y_1 & | & y_2 & | & y_3 & & | & y_n \end{pmatrix} \quad (8)$$

where the supervision state is normalized based on derivation described in Section III, and here, n is the number of qubits; such as $|x_i|^2 + |y_i|^2 = 1$, $i = 1, 2, \cdots, n$. The quantum rotation gate helps to localize the ith bit of the sth individual sensor as q_s is described with Eq. 9.

$$\begin{bmatrix} \widehat{x}_{l,k}^i \\ \widehat{y}_{l,k}^i \end{bmatrix} = \begin{pmatrix} \cos\left(\theta_{l,k}^i\right) & -\sin\left(\theta_{l,k}^i\right) \\ \sin\left(\theta_{l,k}^i\right) & \cos\left(\theta_{l,k}^i\right) \end{pmatrix} \begin{bmatrix} x_{l,k}^i \\ y_{l,k}^i \end{bmatrix} \quad (9)$$

Each state i from 1 to n updates the bit location using the coordinates $\left(\widehat{x_{l,k}^i}, \widehat{y_{l,k}^i} \right)^T$. The rotation angle plays a crucial
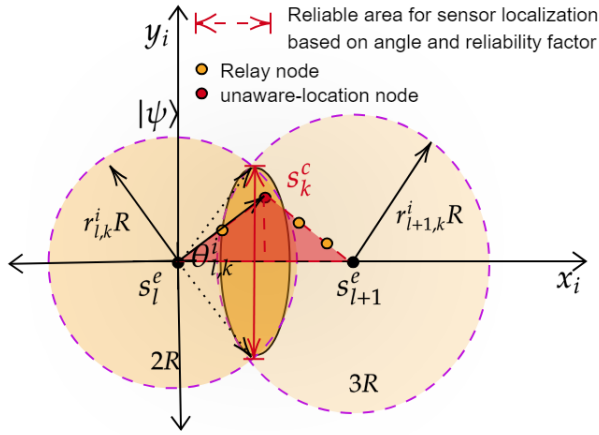
Fig. 3: Vehicle location measurement based on angle and reliability factor

---

Algorithm 1: Node-centric measurement Algorithm

input : s_e^l, $(l = 1, 2, \cdots, L)$ denotes a set GPS enabled sensors, set of hyper nodes s_c^k, $(k = 1, 2, \cdots, K)$

output: Feasible location of relay sensors inline to the active sensors

1 Initialize required attributes $\rho \neq 0$, $R \neq 0$, $d_{l,k} \neq 0$, $\theta_l^k \neq 0$, $s_c = S - s_e$, $\varepsilon \& \varpi \epsilon [0,1]$, $\wp_{s_c} \neq 0$, $\mu_{s_c} \neq 0$;

2 **for** *each $s_l = 1$ to L* **do**

3   **for** *each $s_c = 1$ to K* **do**

4   **if** $l \neq c$ **then**

5   Estimate $\theta_l^k = \hbar \times p(x_i, y_i)$;

6   Estimate $p(x_i, y_i) = \frac{1}{r_{l,k} + r_{l+1,k}} \times \left(\frac{d_{l,k}^{be}}{d_{l,k}^{pre}} \right) \left(\vartheta_{l,k}^{be} - \vartheta_{l,k}^{pre} \right)$ Estimate $d_{l,k} = \int\limits_0^{\theta_{l+1,k}} \frac{r_{l,k} \cdot \alpha_{l,l+1}^k}{\sin \theta_l^k}$;

7   Estimate $\chi = b \left[(O^{pee})^T (O^{pee}) \right]$; # low variance rate is preferred;

8         $s_c[i] \leftarrow$ update the number of top short distance nodes which are equal to its node degree subject to low data variance rate;

9   **end**

10   **else**

11   Update the device position coordinates $s_c(x, y)$ based on Monte Carlo method using cognition coefficient which is $\varpi \neq 0$

12   **if** $\varpi \geq 0.5$ **then**

13   Estimate and update the position $s_c(x_i, y_i) = 0.5 \times (s_c(x_i, y_i) + s_c(x_{i+1}, y_{i+1}))$

14   **end**

15   **else**

16   Update the position $s_c(x_i, y_i) = \varepsilon \times \wp_{s_c} \pm v \times |\wp_{s_c} - \mu_{s_c}| \times \log\left(\frac{1}{\varepsilon}\right)$

17   **end**

18   **end**

19   **end**

20 **end**

---

role in the sensor selection process, determined as follows.

$$\theta_{l,k}^i = \hbar \times p(x_{l.k}^i, y_{l.k}^i)$$

Here, $p(x_{l,k}^i, y_{l,k}^i)$ represents a control function that assesses the direction of rotation. The rotation angle magnitude is denoted by $\hbar_{l,k}^i$. The conditions corresponding to the rotation angle can be found in Table III, which lists all feasible solutions. Figure 3 illustrates the derived position g_s^i and predicted position $\widehat{g_s^i}$ of the relay sensor. Subsequently, a binary solution

TABLE III: Rotation Angle Simulation Outcome

$p(x_{l.k}^i, y_{l.k}^i)$				$\hbar_{l,k}^i$	$f(g_s^i) > f(y_{l.k}^i)$	g_s^i	$\widehat{g}_s^i$
$x_{l.k}^i y_{l.k}^i > 0$	$x_{l.k}^i, y_{l.k}^i < 0$	$x_{l.k}^i = 0$	$y_{l.k}^i = 0$				
0	0	0	0	0	F	0	0
0	0	0	0	0	T	0	0
0	0	0	0	0	F	0	1
+1	-1	0	±1	0.05π	T	0	1
+1	-1	0	±1	0.015π	F	1	0
-1	+1	±1	0	0.030π	T	1	0
-1	+1	±1	0	0.0065π	F	1	1
-1	+1	±1	0	0.0325π	T	1	1

is essential to cross-verify the system's performance. Let us assume that the probability of the current position qubit x_i is compared with a random number ran, $\forall \, 0 \leq ran \leq 1$. The binary solution of the sensor state is defined with Eq. 10.

$$b\left(g_s^i\right) = \begin{cases} 1 & \text{for} \quad |x_i|^2 > ran \\ 0 & \text{for} \quad |x_i|^2 \leq ran \end{cases} \tag{10}$$

The binary solution set is $B = (b_1, b_2, \cdots, b_s)$, $\therefore$ $(s = 1, 2, \cdots S)$ which is derived based on above equation. Algorithm 1 measures the status of hybrid sensors for effective device location through quantum theory. The device deployment at the proper position based on novel measurements affects the system's latency and performance. Unlike the classical method, we design a quantum computing-based node-centric measurement system based on distance, hop count, and coordinates for direction analysis to select the feasible sensor set. In this process, line 1 initializes the demanded attributes, and the selecting node should not be the active node, and lines 5-8 assess the expected position subject to

angle, distance and data variance. The hyper sensor set is updated in ascending order based on the distance and degree of a node/vehicle. Subsequently, the second objective is a resolved-based Algorithm 2. If the hyper node is the same as the active node, then update the location coordinates based on the Monte Carlo method through cognition coefficient weight ϖ. If $\varpi \geq 0.5$, assess the position as follows; else, process line-16. Once the device position is assessed and after that resolves the second target which is based on quantum state estimation as follows

$$s_c(x_i, y_i) = 0.5 \times (s_c(x_i, y_i) + s_c(x_{i+1}, y_{i+1})) \tag{11}$$

B. Fusion variance measurement for quantum state estimation

Quantum state estimation is an essential part of quantum theory which is carried out with three process steps (measurement, analysis and reconstruction) can be observed in Fig 4. Our objective is to strengthen the measurement process because the reconstruction depends on the outcome of the measurement process. The summation of qubit probabilities plays an essential role in finalizing the state of the sensor to accomplish sensor consolidation. Note, enhancing the tomography accuracy means achieving a minimum error rate between
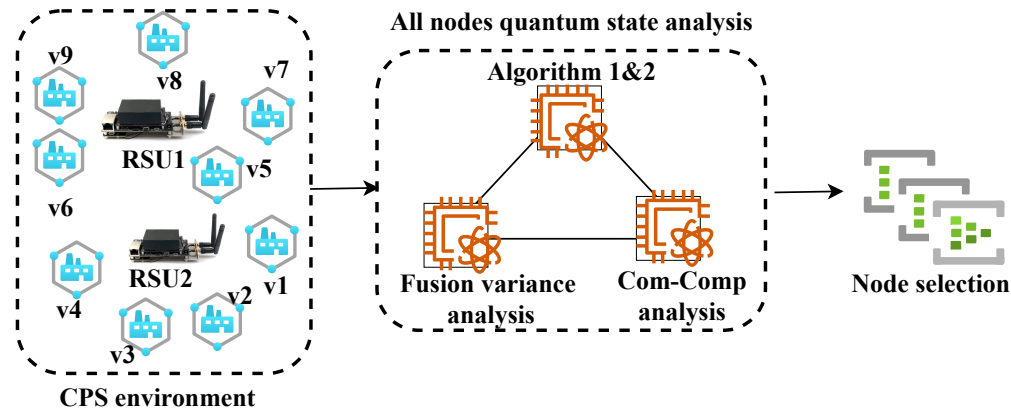
Fig. 4: CPS-based quantum state estimation mechanism

the expected and current true states.

Assuming the quantum state reconstruction as λ, based on n attribute measurements (specifically device contiguity, device optimal knock ratio, and device heterogeneity treated as three qubits), we can define each device as having n channels to collect data for each state. In this context, the operator $\{\pi_i\}_{i=1}^n$ optimizes the measurements of each sensor device, and the current state probability of the ith qubit can be represented as $o_i = tr(\lambda \pi_i)$. To mitigate redundancy and iterative occurrence data, we construct a frequency matrix using a vector $v_i^s(i = 1, 2, \cdots, n; \ s = 1, 2, \cdots, S)$, i.e.,$h_i^s/_{H_s}$, where H_s refer number of reconstruction state of sth device and h_i^s refer total count of ith qubit outcomes. Consequently, the occurrence frequency is estimated as $\sum_s \frac{v_i^s}{S}$, and unbiased true probability vector $O = (o_1, o_2, \cdots, o_m)^T$ is defined as

$$b[V_s] = O \tag{12}$$

The estimation error probability state, denoted as O_s^{pee}, is evaluated as $O_s^{pee} = O - V_s$. The variance matrix of V_s is represented by $\mathbb{C}s = b[O_s^{pee}(O_s^{pee})^T]$, and the covariance matrix between V_s and $Vs+1$ is given by $\mathbb{C}s, s+1 = b[O_s^{pee}(Os+1^{pee})^T]$. In the case where devices s and $s+1$ are independent, $\mathbb{C}_{s,s+1}$ is zero. The sensor weight matrix W_s is defined as follows:

$$[W_1, W_2, \cdots, W_s] \triangleq W \triangleq \left(b^T(\widehat{\mathbb{C}})^{-1}b\right)^{-1} \times (\widehat{\mathbb{C}})^{-1}b \tag{13}$$

where $b = [I_m, \cdots, I_m]^T$ and

$$\widehat{\mathbb{C}} = b\left(\begin{bmatrix} O_1^{pee} \\ \vdots \\ O_S^{pee} \end{bmatrix}\begin{bmatrix} O_1^{pee} \\ \vdots \\ O_S^{pee} \end{bmatrix}^T\right) = \begin{pmatrix} \mathbb{C}_{11} & \cdots & \mathbb{C}_{1S} \\ \vdots & \ddots & \vdots \\ \mathbb{C}_{S1} & \cdots & \mathbb{C}_{SS} \end{pmatrix} \tag{14}$$

Here, b is an identity matrix with an order of b, and $\widehat{c}$ is an error covariance matrix.

Theorem 1. *Let's consider the assessment of the quantum state λ, assuming a total of n attributes. If $\chi = b\left[\left(O - \widehat{O}\right)^T \left(O - \widehat{O}\right)\right] = b\left[(O^{pee})^T (O^{pee})\right]$ represents*

the data fusion variance $\widehat{O}$ then the true data fusion probability $O^{ouf} = \sum_{s=1}^{S} W_s \cdot V_s$ is obtained and the variance matrix $\mathbb{C}^{ouf} \triangleq b\left[\left(O - O^{ouf}\right)^T \left(O - O^{ouf}\right)\right] = \left(b^T(\widehat{\mathbb{C}})^{-1}b\right)^{-1}$ is estimated through linear least mean square error.

Proof. Let's consider a defined method for precisely determining the probability state of a node by integrating unbiased data from sensor nodes as follows

$$O^{ouf} = \sum_{s=1}^{S} W_s \cdot V_s \tag{15}$$

According to the single attribute and multiple attribute fusions, the probabilities are defined as

$$b\left[\sum_{s=1}^{S} W_s \cdot V_s\right] = \sum_{s=1}^{S} W_s \cdot b[V_s] = \sum_{s=1}^{S} W_s \cdot O = O$$

Moreover, we have a true weighting matrix W_s

$$\sum_{s=1}^{S} W_s = I_m \tag{16}$$

Therefore, the data fusion measurement error is redefined as

$$O^{pee} = O - O^{ouf} = \sum_{s=1}^{S} W_s \cdot O_s^{pee} \tag{17}$$

Subsequently, the data fusion variance is similar to $\chi = b\left[(O^{pee})^T (O^{pee})\right]$ and it can be defined as

$$\chi = tr\left(b\left[(O^{pee})^T (O^{pee})\right]\right) = tr(\mathbb{C})$$

Based on Eq. 17, the true variance is as follows

$$b\left[(O^{pee})(O^{pee})^T\right] = b\left[\sum_{s=1}^{S} W_s \cdot O_s^{pee}\left(\sum_{s=1}^{S} W_s \cdot O_s^{pee}\right)^T\right]$$

$$= [W_1, W_2, \cdots, W_s]\, b\left(\begin{bmatrix} O_1^{pee} \\ \vdots \\ O_S^{pee} \end{bmatrix}[O_1^{pee} \cdots O_S^{pee}]\right)\begin{bmatrix} W_1^T \\ \vdots \\ W_S^T \end{bmatrix}$$

$$= W\mathbb{C}W^T \tag{18}$$

As per the above equations $b^T W^T = I_m$, the matrix's can be expressed as follows

$$\begin{bmatrix} \widehat{\mathbb{C}} & b \\ b^T & 0 \end{bmatrix} \begin{bmatrix} W^T \\ Y^T \end{bmatrix} = \begin{bmatrix} 0 \\ I_m \end{bmatrix} \quad (19)$$

According to the above Eq. 19, the matrix is rewritten as

$$\begin{bmatrix} W^T \\ Y^T \end{bmatrix} = \begin{bmatrix} \widehat{\mathbb{C}} & b \\ b^T & 0 \end{bmatrix}^T \begin{bmatrix} 0 \\ I_m \end{bmatrix}$$

$$= \begin{bmatrix} (\widehat{\mathbb{C}})^{-1} b \left(b^T (\widehat{\mathbb{C}})^{-1} b \right)^{-1} \\ -\left(b^T (\widehat{\mathbb{C}})^{-1} b \right)^{-1} \end{bmatrix} \quad (20)$$

Here, $W = \left(b^T (\widehat{\mathbb{C}})^{-1} b \right)^{-1} b^T (\widehat{\mathbb{C}})^{-1}$ is weighting matrix, and $Y^T = -\left(b^T (\widehat{\mathbb{C}})^{-1} b \right)^{-1}$ union matrix. According to Eqs. 15 and 13, and $\mathbb{V} \triangleq \left[V_1^T, V_2^T, \cdots, V_s^T \right]^T$ the true probability is $O^{ouf} = W \times \mathbb{V}$, $b[\mathbb{V}] = \left[O^T \right]_{m \cdot S}^T = bO$, and the legitimated true data fusion probability is

$$b\left[O^{ouf} \right] = \left(b^T (\widehat{\mathbb{C}})^{-1} b \right)^{-1} b^T (\widehat{\mathbb{C}})^{-1} \cdot bO = O \quad (21)$$

$\square$

Corollary 1. *Assume data fusion covariance matrix $\mathbb{C}_{s,s+1} = 1$ when n attributes and s sensors measurements are identical then the O^{ouf} is as follows*

$$O^{ouf} = \sum_{s=1}^{S} W_s \cdot V_s \quad (22)$$

the weighting matrix is defined as

$$W_s = \left(\sum_{s+1}^{S} \mathbb{C}_{s,s+1}^{-1} \right)^{-1} \cdot \mathbb{C}_s^{-1} \quad (23)$$

when the measurements are different, the variance matrix is followed by

$$\mathbb{C}^{ouf} = \left(\sum_{s=1}^{S} \mathbb{C}_s^{-1} \right)^{-1} \quad (24)$$

In case $\mathbb{C}_s > 0$, the Eq. 23 is defined as

$$W_s = I_m - W_s b = I_m - X_s \cdot Z_s^{-1} \quad (25)$$

Thus the Eq. 15 is a conditional true optimal probability, but still, it is quite complex when the sensor measurement attributes dimensions degree is high, and $X_s = [\mathbb{C}_s - \mathbb{C}_{11}, \cdots, \mathbb{C}_s - \mathbb{C}_{1S}]$. However, the following Theorem 2 resolves the data loss and true data fusion issues.

Theorem 2. *According to the variance matrix of V_s is $\mathbb{C}_s = b\left[O_s^{pee} (O_s^{pee})^T \right]$ and the covariance matrix between V_s and V_{s+1} is $\mathbb{C}_{s,s+1} = b\left[O_s^{pee} (O_{s+1}^{pee})^T \right]$, select the data fusion variance $\chi = b\left[(O^{pee})^T (O^{pee}) \right]$ which is estimated as per the sensor performance index, and the sub-optimal true probability is defined as*

$$O_{sub}^{ouf} = \sum_{s=1}^{S} w_s \cdot V_s \quad (26)$$

here the coefficient weights are defined as

$$w = \frac{b^T \cdot \widehat{\mathbb{C}_2}^{-1}}{b^T \cdot \widehat{\mathbb{C}}_2^{-1} \cdot b} \quad (27)$$

based on

$$\widehat{\mathbb{C}}_2 = \begin{pmatrix} tr(\mathbb{C}_{11}) & \cdots & tr(\mathbb{C}_{1S}) \\ \vdots & \ddots & \vdots \\ tr(\mathbb{C}_{S1}) & \cdots & tr(\mathbb{C}_{SS}) \end{pmatrix} \quad b = \begin{pmatrix} 1 \\ \vdots \\ 1 \end{pmatrix}$$

Thus, the weighting coefficients $[w_1, w_2, \cdots, w_S] \triangleq w$ and the variance matrix is written as

$$\mathbb{C}_{sub} = \sum_{s,s+1=0}^{S} w_s \cdot w_{s+1} \cdot \mathbb{C}_{s,s+1} \quad (28)$$

Proof. The single attribute device is called a single measurement device and vice versa. The expected data fusion measurements are considered as follows:

$$b\left[\sum_{s=1}^{S} w_s \cdot V_s \right] = \sum_{s=1}^{S} w_s \cdot b[V_s] = \sum_{s=1}^{S} w_s \cdot O = O \quad (29)$$

Such that,

$$\sum_{s=1}^{S} w_s = 1 \quad (30)$$

The data fusion measurement error is derived as

$$O_{sub}^{pee} = O - O_{sub}^{ouf} = \sum_{s=1}^{S} w_s \cdot O_s^{pee} \quad (31)$$

The subsequent fusion variance matrix is

$$\mathbb{C}_{sub} = b\left[(O^{pee})^T (O^{pee}) \right]$$

$$= \sum_{s,s+1=0}^{S} w_s \cdot w_{s+1} \cdot \mathbb{C}_{s,s+1} \quad (32)$$

and the variance is $\chi_{sub} = tr\left(b\left[(O^{pee})(O^{pee})^T \right] \right) \triangleq tr(\mathbb{C}_{sub})$. According to Eq. 20, an increase in the number of qubits resulted in a corresponding increase in the computational complexity. Consequently, the measurement of each sensor state's probability becomes more complex when there is an increase in attributes or qubits during a state assessment. However, our gradient model helps improve computational efficiency despite these complexities. $\square$

Corollary 2. *If the values of n attributes and s sensor measurements do not match, the covariance matrix $\mathbb{C}_{s,s+1}$ for data fusion is assumed to be zero. In this case, the value of O^{ouf} can be determined as follows.*

$$O_{sub}^{ouf} = \sum_{s=1}^{S} w_s \cdot V_s \quad (33)$$

Legitimately, we have weight matrix

$$w_s = \left(\sum_{s=1}^{S} \frac{1}{tr(\mathbb{C}_{s+1})} \right)^{-1} \times \frac{1}{tr(\mathbb{C}_s)}$$

and the corresponding variance matrix is defined as

$$\mathbb{C}_s = \sum_{s=1}^{S} w_s^2 \cdot \mathbb{C}_s \tag{34}$$

Subsequent variance is calculated as

$$\chi_{sub} = tr\left(\mathbb{C}_{sub}\right) = \left(\sum_{s=1}^{S} \frac{1}{tr\left(\mathbb{C}_{s+1}\right)}\right)^{-1} \tag{35}$$

Proof. For $\mathbb{C}_{s,s+1} = 0$ $(s \neq s+1)$, we have

$$\widehat{\mathbb{C}}_2^{-1} = diag\left[\frac{1}{tr\left(\mathbb{C}_1\right)}, \frac{1}{tr\left(\mathbb{C}_2\right)}, \cdots, \frac{1}{tr\left(\mathbb{C}_S\right)}\right] \tag{36}$$

By substituting the aforementioned equation, the resulting weight and variance matrix can be obtained as follows.

$$w_s = \left(\sum_{s=1}^{S} \frac{1}{tr\left(\mathbb{C}_{s+1}\right)}\right)^{-1} \cdot \frac{1}{tr\left(\mathbb{C}_s\right)} \tag{37}$$

$$\mathbb{C}_s = \sum_{s,s+1=0}^{S} w_s w_{s+1} \cdot \mathbb{C}_{s,s+1} = \sum_{s=1}^{S} w_s^2 \cdot \mathbb{C}_s \tag{38}$$

Consequently, the estimated variance of data fusion for each measurement is calculated as follows.

$$\begin{aligned}
\chi_{sub} &= tr\left(\mathbb{C}_{sub}\right) \\
&= \sum_{s=1}^{S} w_s^2 \cdot tr\left(\mathbb{C}_s\right) \\
&= \sum_{s=1}^{S} \left(\sum_{s=1}^{S} \frac{1}{tr\left(\mathbb{C}_s\right)}\right)^{-2} \cdot \frac{1}{\left(tr\left(\mathbb{C}_s\right)\right)^2} \cdot tr\left(\mathbb{C}_s\right) \\
&= \left(\sum_{s=1}^{S} \frac{1}{tr\left(\mathbb{C}_s\right)}\right)^{-2} \cdot \sum_{s=1}^{S} \frac{1}{tr\left(\mathbb{C}_s\right)} \\
&= \sum_{s=1}^{S} \frac{1}{tr\left(\mathbb{C}_s\right)}
\end{aligned} \tag{39}$$

□

The developed fusion mechanism, utilizing scalar and matrix weighting coefficients, is based on linear least mean square error. This mechanism aims to differentiate the probability of each qubit and estimate the potential of the sensor to address computation and communication overhead challenges associated with sensor states. The diagonal elements of $\mathbb{C}_s$ are utilized to indicate the measurement accuracy of device s. Algorithm 2 assesses the quantum state to select the RSU or server by measuring node contiguity, node optimal knack rate, and node heterogeneity parameters. In this process, line 1 initializes three quantum bits (contiguity ratio, knack ratio, and heterogeneity weight). Moreover, each node's fitness weight is estimated before its selection. Line 4 assesses the contiguity ratio, and line 6 assesses the knack ratio and heterogeneity weight with line 7. The detailed quantum state estimation is derived in the below Subsection IV-B1, which helps to conclude the quantum register state with probability ratio. As per the demand of qubits, the vehicle would be selected. The fitness function is applied to select the sensor if $\eta_s \geq 0.5$.
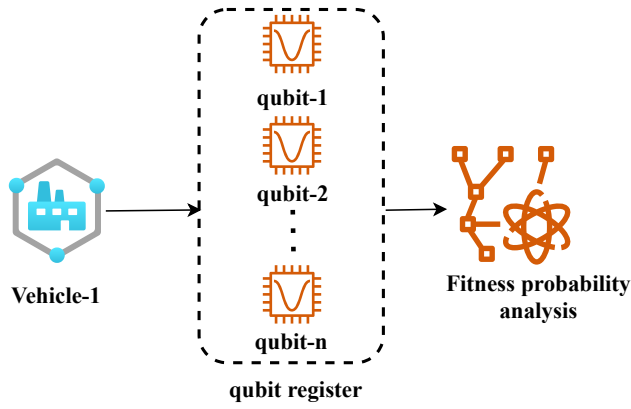

Algorithm 2: Quantum state estimation algorithm to select sensor

input : Potential sensor list $s_c[i] \neq 0$,
$Q = (q_1, q_2, \cdots, q_s, \cdots, q_n)$
output: Select feasible sensor
1 Initialize required attributes $\xi_{s_c} \neq 0$, $\gamma_{s_c} \neq 0$, $\chi_{s_c} \neq 0$;
2 **for** *each $s_c[i] = 1$ to n* **do**
3   **#contiguity ratio assessment#**
4   Estimate $\sqrt{\frac{S}{6A/\pi}} \leftarrow R$, where $|d_{l,k}| < R$ and $R_t \geq 2R_s$ to assess the concerning node contiguity ratio ξ_{s_c} and $\rho\left(\xi_{s_c}\right)$;
5   **#optimal knack ratio assessment#**
6   Estimate $\gamma_{s_c} = \frac{\text{total demanded resources}}{\text{total available resources}}$ and its probability;
7   Estimate φ_{s_c} using Eq. 41;
8   Update node heterogeneity and non-linearity;
9   **#likelihood probability and fitness assessment**
10   Measure & update the likelihood probability of each sensor through T-gate based on Subsection IV-B1.
11   Update $s_{c[i]}$ ascending order as per probability;
12   Estimate the fitness $\eta_s = \rho\left(\xi_{s_c} \mid \gamma_{s_c}, \varphi_{s_c}\right) \times \sum_{m=1}^{6}\left(\sqrt{C_m}\right)$;
13   **if** $\eta_s \geq 0.5$ **then**
14   Select the sensor as potentially computation rich;
15   **end**
16   **else**
17   Check the rest of the sensors until the stack value reaches zero; else go-to step 2;
18   **end**
19 **end**

---

1) Iterative data fusion analysis using quantum gates: To assess the quantum register state of each, we used a series of gates to manipulate the qubits in the register and then measure the resulting state, including T-gate and H-gate. The *H-gate* suits individual qubits within the register to construct a balanced mixture of computational basis states, making it easier to probe and analyze the quantum state. The resulting superposition states can be measured to obtain statistical information about the quantum register's state. The *T-gate* is a fundamental gate used for phase estimation. T-gate is employed on selected qubits to adjust the relative phases between the qubits' superposition states. This phase control is vital for performing accurate quantum calculations and extracting meaningful results.

In our simulation, three qubits are considered. To create a superposition in a single qubit, we used H−gate to the qubit for a lightweight environment. This puts the qubit in a state where it has a 50% chance of being in the $\mid 1\rangle$ state and a 50% chance of being in the $\mid 0\rangle$ state. For complex environment calculations, we combined multiple gates, including T−gates and H−gates, in a controlled and coherent manner to help the quantum state to map the classical states (0 or 1).

The probability-based normalization process is employed while assessing the qubit's state. In continuation, let's assume three qubits with eight dimensions, and the best dimension for the node probability determines which node is chosen.

$$|\psi_{s_c}\rangle = \frac{1}{\sqrt{5}}|110\rangle + \sqrt{\frac{1}{5}}|101\rangle - \sqrt{\frac{2}{5}}|011\rangle + \sqrt{\frac{1}{5}}|111\rangle.$$

To complete the node selection, let us assume that the first

This article has been accepted for publication in IEEE Transactions on Network Science and Engineering. This is the author's version which has not been fully edited and content may change prior to final publication. Citation information: DOI 10.1109/TNSE.2023.3301402

IEEE TRANSACTION ON NETWORK SCIENCE AND ENGINEERING, VOL. XX, NO. XX, XXX 2023
10

Fig. 5: The node/vehicle state consolidation involves analyzing the probability variance through quantum-based data fusion

qubit has an elevated weight, meaning that the 1st bit is equal to 1, and the corresponding probability is

$$= \left| \tfrac{1}{\sqrt{5}} \right|^2 + \left| \sqrt{\tfrac{1}{5}} \right|^2 + \left| \sqrt{\tfrac{1}{5}} \right|^2 = 0.2 + 0.2 + 0.2 = 0.6$$

However, their probability is not equal to 1; therefore, we apply the normalization formula as follows by dividing them by their probability.

$$= \frac{\tfrac{1}{\sqrt{5}}|110\rangle - \sqrt{\tfrac{2}{5}}|011\rangle + \sqrt{\tfrac{1}{5}}||111\rangle}{2 \big/ \sqrt{5}} = \tfrac{1}{2}|110\rangle - \tfrac{1}{\sqrt{2}}|011\rangle + \tfrac{1}{2}|111$$

Now the normalization factor is

$$= \left| \tfrac{1}{2} \right|^2 + \left| \tfrac{1}{\sqrt{2}} \right|^2 + \left| \tfrac{1}{2} \right|^2 = 0.2 + 0.5 + 0.2 = 1$$

It confines that, the 3-qubit quantum register is in $|\psi_{s_c}\rangle = \tfrac{1}{2}|110\rangle - \tfrac{1}{\sqrt{2}}|011\rangle + \tfrac{1}{2}|111\rangle$. Figure 5 illustrates each sensor's data fusion analysis, which plays an important role in assessing the sensor state. T-gate and H-gate are considered to assess the quantum register state at each iteration based on Algorithm-1 and Algorithm-2. Figure 6(a) illustrates the probabilities of each dimension, as per the demand and weight of qubit, the sensor would be selected, and detailed simulation outcomes are described in Section V.

C. Node selection strategy based on conditional probability

To evaluate the state of a node, a node selection strategy is employed, which relies on the conditional probability of each constraint mentioned earlier. For instance, the fusion variance probability value must fulfill the constraint C_6 to be considered in the node state estimation process.

$$s_j \mid state\rangle = \sqrt{\chi_s^{pe}} \, |\rangle 1 + \sqrt{1 - \chi_s^{pe}} \, |\rangle 0$$

Likewise, a matrix can be formed in the following manner, with a value of 1 representing node selection and any other value indicating non-selection, prompting the non-selection case to restart the process. For more information please refer [24], [28].

$$S_j^{time} = \begin{bmatrix} 1 \leftarrow \sqrt{C_1} \mid & \cdots & \sqrt{C_6} \mid \\ 0 \leftarrow \sqrt{1 - C_1} \mid & \cdots & \sqrt{1 - C_6} \mid \end{bmatrix}$$

Subsequently, node fitness probability is estimated as follows, where m indicates the number of constraints defined in the problem formulation section.

$$\eta_s = \rho \left(\xi_{s_c} \mid \gamma_{s_c}, \varphi_{s_c} \right) \times \sum_{m=1}^{6} \left(\sqrt{C_m} \right) \qquad (40)$$

1) Vehicle mobility impact on node selection: The primary reason for the lack of success in service offloading objectives is the high mobility of vehicles, leading to data transmission failures or disturbances when the unusual server's execution time. Therefore, ensuring a short transmission time for the link has become significant, and the short transmission link time is derived as follows.

$$\varphi_{j,j+1|j,k} = \begin{cases} \frac{R + d_{j,j+1|k}}{|\varkappa_j - \varkappa_{j+1|k}|} & \text{for} \quad \varkappa_j > \varkappa_{j+1|k} \\ \frac{R + d_{j,j+1|k}}{|\varkappa_j + \varkappa_{j+1|k}|} & \text{for} \quad \varkappa_j \leq \varkappa_{j+1|k} \end{cases} \qquad (41)$$

When the direction of vehicles is not the same, the transmission channel link quality

$$\varphi_{j,j+1|j,k} = \frac{\sqrt{R^2 - (y_j - y_{j+1|k})} + d_{j,j+1|k}}{|\varkappa_j + \varkappa_{j+1|k}|} \qquad (42)$$

where $\varphi_{j,j+1|j,k}^{\tau}$ is transmission link between j^{th} vehicle, $j + 1^{th}$ vehicle or between j^{th} vehicle, k^{th} server over the network. Here, d_j is the speed of jth vehicle, R indicates coverage range, ϖ_j, $\varpi_{j+1|k}$ is the distance between vehicles and server, respectively; In this scenario, we select the offloading node based on a specific condition: the probability of service execution elapsed time being less than the probability of transmission link time.

D. Complexity analysis

In the proposed mechanism, the calculation of each vehicle/node state, denoted as $|S\rangle$, is crucial since the selection of nodes relies on the probability of node dimension. Therefore, the probability amplitude of the node state must be equal to one, expressed as $\sum_{s=1}^{S} | b_s |^2 = 1$. The evaluation involves assessing the suitable vehicle or node across its state spaces N, performing iterative search actions with l number of vehicles, q control qubits which can observe in Algorithm 1 and 2. As a result, the complexity of the proposed approach can be represented as $\mathcal{O} \left(\sqrt{N^l} I^l \cdot q \, log \, q \right)$, which encompasses weight summation, searching, and estimation of all parameters. *Space complexity:* Typically, the required qubit storage for a node is proportional to the logarithm of the number of conditional qubits, denoted as $\mathcal{O} \left(\log q \right)$.

V. EXPERIMENTAL RESULTS

In this Section, the simulation results are plotted to determine the performance of our system. The Rigetti forest cloud platform and QUBIT4MATLAB V5.8 with MATLAB are used to evaluate every numerical simulation. The PyQuil package is used by Rigetti's forest cloud platform to simulate our method in a quantum virtual environment. $H()$: Hadamard gate, $R()$: Ration gate, $T()$: t-gate, $I()$: Identity gate have

used in the simulation. Additionally, on 64-bit Ubuntu 20.1 LTS with an Intel Core i7-10700 CPU running at 3.80GHz and an NVIDIA GeForce RTX3090, the Qiskit tool is utilized for cross-verification. The state-of-art (SOTA) approaches are labelled QAOA(A1), Q-Ebit(A2), and NDQ(A3), where A1 is a novel quantum service allocation model [16]. A2 is a quantum-inspired communication and computation framework [9]. A3, a quantum-based swarm optimization algorithm [8].

In our simulation, a backhaul link with a 10 Gb capacity connects c=3,6,9 RSUs and 31% of vehicles for efficient communication and processing. The MATLAB function generates Rayleigh fading channel value, and the channel bandwidth is fixed as 1000Hz. There are eight actions and six states for 3-qubits, respectively. The full-duplex node deployment helps to preserve channel resource usage and communication delay, and the simulation variables are listed in Table IV. The compute service's anticipated storage size is 15 Mb, and the plots are built using 300 iterations of the logs and a CPU cycle per bit.

Figure 6 illustrates the state estimation analysis based on the dimensions of each qubit and mean distance error analysis. Quantum-based probability estimation helps to finalize the state of each vehicle. According to that, the value vehicle selection takes place, which impacts the system's performance in terms of low delay, resource usage, and quality of experience. To choose the RSU server by the application deadline, our two algorithms evaluate the node position using rotation angle and h-gate. Each dimension probability of a single sensor's qubit register is shown in Figure 6(a). Moreover, the first two qubits have been assigned a higher priority than the third qubit using weight because the first two significantly impact the system performance. Consequently, the probability ratio is plotted for all four sensors as represented in Figure 6(b). The first aim of this paper is to assess the suitable position of the sensor to meet the qualitative coverage ratio and to cover the sensor service demands concerning distance estimation and angle measurement. Therefore, the mean distance error is assessed and plotted concerning dimensions and sensor count, which can be observed in Figure 6(c). The proposed method achieved a lower error rate than SOTA approaches, even at different dimensional levels.

Figure 7 illustrates service rate analyses of the proposed method. We considered three different scenarios to assess the proposed system's performance. Usually, sensor density, service arrival rate, and coverage range affect the service reliability rate, and three variables vary per the service demand to meet the application deadline. We noticed that, as the computation and communication capacity increased, the anchor count and the service execution ratio drastically increased, as can be observed from Figure 7(a) to Figure 7(c).

Figure 8 illustrates the qubit dimension impact on system performance. Figure 8(a) shows demanded time to complete each iteration concerning dimension count. The proposed system achieved a low consumption time which is an average of 1.1k seconds. Consequently, A1, A2, and A3 achieved an average time computation rate. Figure 8(b) shows the node-selection error rate based on dimension probability. In this

case, the proposed model achieved low error rate than the rest of the methods since our state estimation method adequately measures the states and their probability for concluding the device selection process. In addition to that, fitness value is also estimated and considered before selecting the suitable sensor. The concerning fitness values of each sensor based on dimensions are plotted in Figure 8(c).

Figure 9 illustrates the error ratio concerning service coverage and resource usage analysis. The proposed system achieved a low normalized root mean square error of around 0.29% than SOTA approaches concerning the increase of hypernode count, which can be observed in Figure 9(a). Deploying the sensor at the right position impacts the service reliability ratio, which mitigates the system's coverage issues. The proposed method achieved a high coverage ratio by fulfilling resource requirements with less communication and computation overhead, as shown in Figure 9(b). In continuation, maintaining a trade-off between resource usage cost and latency minimization over joint computation and communication. The proposed method achieved low resource usage concerning the increment in hypernode count, which can be observed in Figure 9(c).

TABLE IV: The simulation parameters include coverage range (CR), transmission power (TP), channel frequency (CF), and thermal noise power (TNP), bandwidth (B).

| variable	value	variable	value
RSU		**OBU**	
coverage	300m	**coverage**	150m
CF	6 GHz	**CF**	4 GHz
TP	50 dBm	**TP**	30 dBm
B	50 MHz	**B**	15 MHz
variable		**Value**	
size		15Mb	
distance		160 m	
TNP		-91 dBm	
time variance		5.3×10^{-4}s	
ω_h		0.5	
Γ_h		3.6/unit	
$\mathbb{O}$		26	
density		5-6/km	

Two scenarios have been considered and corresponding results amended in Table V. The second case, specifically shows a deficient infrastructure, making it difficult to combine low error and latency rates with high service reliability. The creation of a novel node consolidation system by taking into account the qubit register probability and quantum machine

TABLE V: Performance analysis in both scenario-1: 8 vehicles, 4 RSUs, 30% service arrival rate as well as scenario-2: 12 vehicles, 2 RSUs, 60% service arrival rate

#Scenario-1			
Method	**Service reliability %**	**Consolidation error rate %**	**Offloading reduction %**
NDQ(A3[8])	29.2	0.46	26.2
Q-Ebit(A2[9])	30.6	0.41	48.5
DQRA(A1[16])	34.1	0.35	49.3
QONC	**36.7**	**0.17**	**53.1**
#Scenario-2			
Method	**Service reliability %**	**Consolidation error rate %**	**Offloading reduction %**
NDQ(A3[8])	61.2	0.53	49.6
Q-Ebit(A2[9])	67.5	0.79	56.3
DQRA(A1[16])	68.7	0.72	62.1
QONC	**70.2**	**0.22**	**74.3**
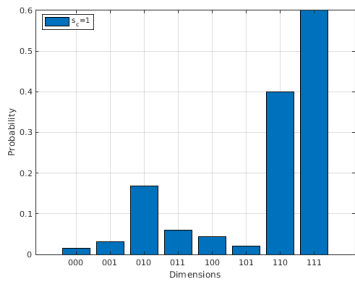
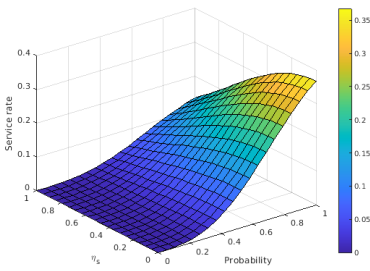(a) Single sensor state probability based on dimension
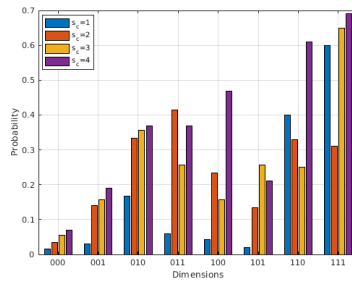
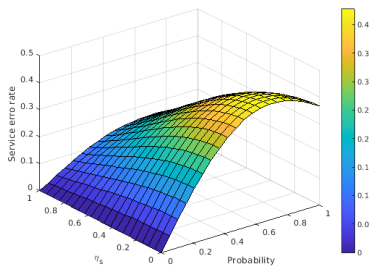(b) Multi-node state probability analysis based on dimensions
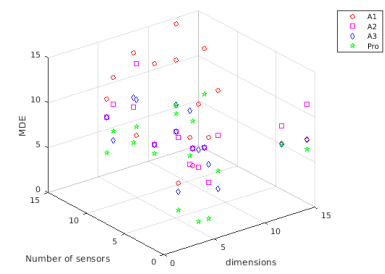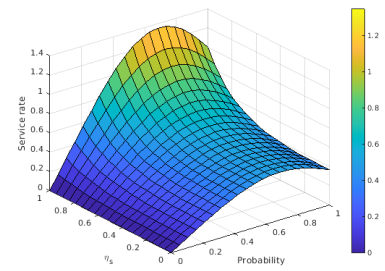
(c) Mean distance error analysis

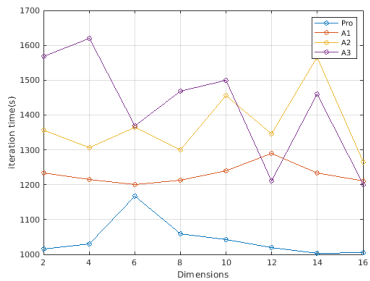Fig. 6: Sensor state analysis

(a) Service rate when anchors=3

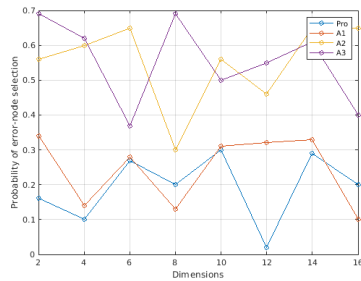(b) Service rate when anchors=6
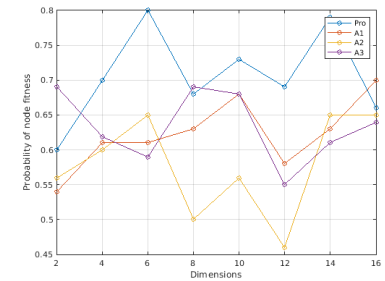
(c) Service rate when anchors=9

Fig. 7: Server/RSU service rate analysis when sensor density=31%,, service arrival rate=49%, coverage range=500m

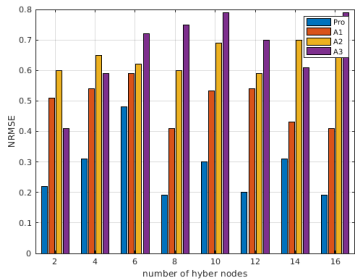(a) Required time for completing each iteration

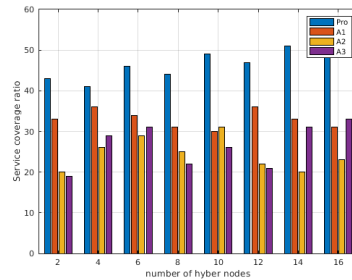(b) Node selection probability error rate analysis
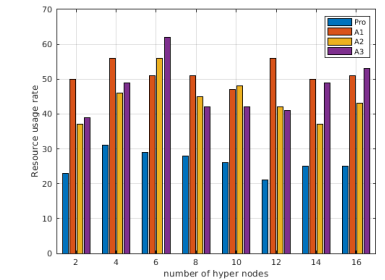
(c) Fitness analysis for node selection

Fig. 8: Performance analysis using Qubit dimensions

(a) Normalized root mean square error analysis

(b) Service coverage ratio analysis

(c) Resource usage analysis

Fig. 9: Node density based on error ratio, resource usage, and service coverage analysis

TABLE VI: Quantum-based node consolidation mechanism; Er: error rate, Fre: frequency, Ct: completion time, wt: waiting time, Dec: decision

# Devices	Qubits probability			Er	Fre(GHz)	Ct (ms)	wt(ms)	Dec
	$\lvert 110\rangle$	$\lvert 101\rangle$	$\lvert 111\rangle$					
$l_a\lvert\rangle$	0.62	0.71	0.75	0.6	7.2	5.2	520	not suitable
$l_b\lvert\rangle$	**0.6**	**0.65**	**0.78**	**0.21**	**6**	**3.1**	**789**	**SR vehicle**
$l_c\lvert\rangle$	0.70	0.69	0.72	0.71	8.1	4.9	825	not suitable
$l_d\lvert\rangle$	**0.75**	**0.79**	**0.82**	**0.15**	**3.1**	**1.5**	**315**	**Suitable**

learning mechanism led to the proposed's low latency and error rate. The fitness weight prediction function is crucial for maintaining a trade-off between resource usage, coverage ratio, and latency rate while choosing the best RSU. First, let's imagine that there are four servers in a CPS framework, each with a separate set of computational resources, and that server $l_b\lvert range$ is overloaded as a result of a high service arrival rate. In this scenario, offloading takes place by node, which is chosen based on the node-centric characteristics stated in Table. VI.

According to a set of measurements (node contiguity, node heterogeneity, and node optimal knack rate), including quantum state estimation and data fusion optimization, the red tuple offloads the services to the appropriate node in blue. In short, while accommodating the offloaded services, the targeted node service frequency, waiting time relative to the service length, and execution time are also crucial. The blue tuple was chosen because it may be resource-rich for computing. The system performance improves more with this selection strategy than with SOTA methods.

VI. CONCLUSION

This paper develops a QONC decision-making system to select a feasible node to meet application latency constraints and to deploy the node at the appropriate position for accurate data computation-communication. The angular-based node position analysis method effectively localized the node position, which is essential to achieving low latency and enhancing system performance. The simulation results show that our method has achieved a low average error ratio from 0.17-0.22 and an average coverage ratio from 29%-42% because of estimating quantum-formalized node parameters (node contiguity, node optimal knack rate, node heterogeneity). The proposed model achieved 74.3% offloading reduction accuracy, and a 70.2% service reliability rate. The designed fitness function assesses the node fitness probability before selecting the potential device to execute the offloaded services. To satisfy the needs of applications with tight deadlines, we will expand on this work in the future by developing intelligent decision-making methods using linear programming and the Grovers algorithm.

VII. FUTURE OBJECTIVES

The advantage of designing a Quantum Reinforcement Learning (QRL) over traditional RL is carried out by three strategies,

1) The equilibrium ratio between exploration and exploitation of actions will be achieved in QRL's exploration policy,

which will be based on the collapse postulate rather than the greedy or Boltzmann policies.

2) Designing and utilizing the unitary transformation method in a coordinated manner, the QRL model will update all of the states concurrently.

3) The robust nature of the QRL algorithm will help adapt to different learning rates quickly as the unknown changes in the environment.

The robust nature of the QRL approach will be evaluated through learning performance and convergence rate analysis in certain simulations for lightweights and complex environments in the future.

REFERENCES

[1] J. Lee, B. Bagheri, and H.-A. Kao, "A cyber-physical systems architecture for industry 4.0-based manufacturing systems," *Manufacturing letters*, vol. 3, pp. 18–23, 2015.

[2] K. Cao, S. Hu, Y. Shi, A. W. Colombo, S. Karnouskos, and X. Li, "A survey on edge and edge-cloud computing assisted cyber-physical systems," *IEEE Transactions on Industrial Informatics*, vol. 17, no. 11, pp. 7806–7819, 2021.

[3] J. Villalba-Diez and X. Zheng, "Quantum strategic organizational design: alignment in industry 4.0 complex-networked cyber-physical lean management systems," *Sensors*, vol. 20, no. 20, p. 5856, 2020.

[4] C. Cicconetti, M. Conti, and A. Passarella, "Request scheduling in quantum networks," *IEEE Transactions on Quantum Engineering*, vol. 2, pp. 2–17, 2021.

[5] F. Xiao, W. Liu, Z. Li, L. Chen, and R. Wang, "Noise-tolerant wireless sensor networks localization via multinorms regularized matrix completion," *IEEE Transactions on Vehicular Technology*, vol. 67, no. 3, pp. 2409–2419, 2017.

[6] Y. Wang and K. Ho, "Unified near-field and far-field localization for aoa and hybrid aoa-tdoa positionings," *IEEE Transactions on Wireless Communications*, vol. 17, no. 2, pp. 1242–1254, 2017.

[7] N. Patwari, J. N. Ash, S. Kyperountas, A. O. Hero, R. L. Moses, and N. S. Correal, "Locating the nodes: cooperative localization in wireless sensor networks," *IEEE Signal processing magazine*, vol. 22, no. 4, pp. 54–69, 2005.

[8] S. N. Ghorpade, M. Zennaro, B. S. Chaudhari, R. A. Saeed, H. Al-humyani, and S. Abdel-Khalek, "Enhanced differential crossover and quantum particle swarm optimization for iot applications," *IEEE Access*, vol. 9, pp. 93 831–93 846, 2021.

[9] S. Kumar, O. Kaiwartya, M. Rathee, N. Kumar, and J. Lloret, "Toward energy-oriented optimization for green communication in sensor enabled iot environments," *IEEE Systems Journal*, vol. 14, no. 4, pp. 4663–4673, 2020.

[10] L. Tello-Oquendo, S.-C. Lin, I. F. Akyildiz, and V. Pla, "Software-defined architecture for qos-aware iot deployments in 5g systems," *Ad Hoc Networks*, vol. 93, p. 101911, 2019.

[11] N. Saeed, A. Celik, M.-S. Alouini, and T. Y. Al-Naffouri, "Performance analysis of connectivity and localization in multi-hop underwater optical wireless sensor networks," *IEEE Transactions on Mobile Computing*, vol. 18, no. 11, pp. 2604–2615, 2018.

[12] X. Wang, C. Chen, M. Jiang, and X. Huang, "Quantum network coding for remote state preparation of multi-qudit states," in *2019 IEEE International Conference on Systems, Man and Cybernetics (SMC)*. IEEE, 2019, pp. 1150–1153.

[13] D.-D. Li, F. Gao, S.-J. Qin, and Q.-Y. Wen, "Perfect quantum multiple-unicast network coding protocol," *Quantum Information Processing*, vol. 17, no. 1, pp. 1–18, 2018.

[14] S. Dai, M. Liwang, Y. Liu, Z. Gao, L. Huang, and X. Du, "Hybrid quantum-behaved particle swarm optimization for mobile-edge computation offloading in internet of things," in *International Conference on Mobile Ad-Hoc and Sensor Networks*. Springer, 2017, pp. 350–364.

[15] S.-Y. Kuo, Y.-H. Chou, and C.-Y. Chen, "Quantum-inspired algorithm for cyber-physical visual surveillance deployment systems," *Computer Networks*, vol. 117, pp. 5–18, 2017.

[16] J. Yao, M. Bukov, and L. Lin, "Policy gradient based quantum approximate optimization algorithm," in *Mathematical and Scientific Machine Learning*. PMLR, 2020, pp. 605–634.

[17] L. Le and T. N. Nguyen, "Dqra: Deep quantum routing agent for entanglement routing in quantum networks," *IEEE Transactions on Quantum Engineering*, vol. 3, pp. 1–12, 2022.

[18] Q. Tu, Y. Zhao, and X. Liu, "Recovery schemes of hop count matrix via topology inference and applications in range-free localization," *Expert Systems with Applications*, vol. 200, p. 116906, 2022.

[19] M. Jemmali, M. Denden, W. Boulila, G. Srivastava, R. H. Jhaveri, and T. R. Gadekallu, "A novel model based on window-pass preferences for data emergency aware scheduling in computer networks," *IEEE Transactions on Industrial Informatics*, vol. 18, no. 11, pp. 7880–7888, 2022.

[20] K. Li, Z. Huang, and Z. Jia, "Rahg: A role-aware hypergraph neural network for node classification in graphs," *IEEE Transactions on Network Science and Engineering*, 2023.

[21] F. Han and X. Liu, "Anchor-pairs conditional decision-based node localization for anisotropic wireless sensor networks," in *2019 IEEE 11th International Conference on Communication Software and Networks (ICCSN)*, 2019, pp. 84–88.

[22] P. K. Rai, H. Idsøe, R. R. Yakkati, A. Kumar, M. Z. Ali Khan, P. K. Yalavarthy, and L. R. Cenkeramaddi, "Localization and activity classification of unmanned aerial vehicle using mmwave fmcw radars," *IEEE Sensors Journal*, vol. 21, no. 14, pp. 16 043–16 053, 2021.

[23] A. El Assaf, S. Zaidi, S. Affes, and N. Kandil, "Robust anns-based wsn localization in the presence of anisotropic signal attenuation," *IEEE Wireless Communications Letters*, vol. 5, no. 5, pp. 504–507, 2016.

[24] M. Mekala, G. Srivastava, J. C.-W. Lin, G. Dhiman, J. H. Park, and H.-Y. Jung, "An efficient quantum based d2d computation and communication approach for the internet of things," *Optical and Quantum Electronics*, vol. 54, no. 6, pp. 1–19, 2022.

[25] D. Kudrow, K. Bier, Z. Deng, D. Franklin, Y. Tomita, K. R. Brown, and F. T. Chong, "Quantum rotations: a case study in static and dynamic machine-code generation for quantum computers," in *Proceedings of the 40th Annual International Symposium on Computer Architecture*, 2013, pp. 166–176.

[26] M. S. Mekala, G. Dhiman, G. Srivastava, Z. Nain, H. Zhang, W. Viriyasitavat, and G. P. S. Varma, "A drl-based service offloading approach using dag for edge computational orchestration," *IEEE Transactions on Computational Social Systems*, pp. 1–9, 2022.

[27] M. S. Mekala, A. Jolfaei, G. Srivastava, X. Zheng, A. Anvari-Moghaddam, and P. Viswanathan, "Resource offload consolidation based on deep-reinforcement learning approach in cyber-physical systems," *IEEE Transactions on Emerging Topics in Computational Intelligence*, vol. 6, no. 2, pp. 245–254, 2022.

[28] M. S. Mekala, H. Zhang, J. H. Park, and H.-Y. Jung, "Quantum-based offloading strategy for intelligent vehicle network," in *2023 IEEE 20th Consumer Communications & Networking Conference (CCNC)*, 2023, pp. 987–988.

Gautam Srivastava Gautam Srivastava is a Professor of Computer Science at Brandon University, Canada. In his 10- year academic career, he has published a total of 400 papers in high-impact conferences in many countries and high-status journals (SCI, SCIE). He is an Editor of several international scientific research journals including IEEE Transactions on Industrial Informatics, IEEE Transactions on Computational Social Systems, and IEEE Internet of Things Journal. He received his M.Sc. (2006) and Ph.D. (2012) in Computer Science from the University of Victoria, Canada.

Amir H. Gandomi is a Professor of Data Science and an ARC DECRA Fellow at the Faculty of Engineering & Information Technology, University of Technology Sydney. Prior to joining UTS, Prof. Gandomi has published 350+ journal papers and 14 books which collectively have been cited 43,000+ times (H-index = 93). He has been named as one of the most influential scientific minds and received the Highly Cited Researcher award (top 1% publications and 0.1% researchers) from Web of Science for six consecutive years, from 2017 to 2022.

Ju H. Park (Senior Member, IEEE) received the Ph.D. degree in electronics and electrical engineering from Pohang University of Science and Technology (POSTECH), Pohang, Republic of Korea, in 1997. He joined Yeungnam University, Kyongsan, Republic of Korea, in March 2000, where he is currently the Chuma Chair Professor. He has published a number of articles in these areas. His research interests include robust control and filtering, neural/complex networks, fuzzy systems, multiagent systems, and chaotic systems. Since 2015, he has been a recipient of the Highly Cited Researchers Award by Clarivate Analytics (formerly, Thomson Reuters) and listed in three fields, Engineering, Computer Sciences, and Mathematics, in 2019 to 2022.

M. S. Mekala (Senior Member, IEEE, AFHE) received the Ph.D. degree from VIT University. He is currently working as an Assistant Professor with the School of Computing, Robert Gordon University, Aberdeen, U.K. He is a Former Post-Doctoral Researcher at RLRC LAB, Yeungnam University, Gyeonnsan, Korea. His research interests include service computing, intelligent machine vision, data communication, decision making system design, edge computing, CPS, IoT communication, and Reliability Analysis.

Ho-Youl Jung received the Ph.D. degree in electronics engineering from the INSA de Lyon (Institute National des Sciences Appliquées de Lyon), France, in 1998. He is currently a Professor with the Department of Information and Communication Engineering, Yeungnam University, Korea. His research interests include digital signal processing, computer vision, deep-learning, autonomous vehicle, computer graphics, control signal processing, and IoT.